Arch Appl Mech (2005) 74: 808–819
DOI 10.1007/s00419-005-0409-2

ORIGINAL

K. Naumenko · H. Altenbach

A phenomenological model for anisotropic creep in a multipass weld metal

Received: 14 January 2005 / Accepted: 23 May 2005 / Published online: 21 October 2005

Abstract Creep strength of welded joints can be estimated by continuum damage mechanics. In this case constitutive equations are required for different constituents of the welded joint: the weld metal, the heat-affected zone, and the parent material. The objective of this paper is to model the anisotropic creep behavior in a weld metal produced by multipass welding. To explain the origins of anisotropic creep, a mechanical model for a binary structure composed of fine-grained and coarse-grained constituents with different creep properties is introduced. The results illustrate the basic features of the stress redistribution and damage growth in the constituents of the weld metal and agree qualitatively with experimental observations. The structural analysis of a welded joint requires a model of creep for the weld metal under multiaxial stress states. For this purpose the engineering creep theory based on the creep potential hypothesis, the flow rule, and assumption of transverse isotropy is applied. The outcome is a coordinate-free equation for secondary creep formulated in terms of the Norton–Bailey–Odqvist creep potential and three invariants of the stress tensor. The material constants are identified according to the experimental data presented in the literature.

Keywords Weld metal · Multipass welding · Anisotropic creep

1 Introduction

For many structures designed for high-temperature applications, e.g., piping systems and pressure vessels, an important problem is the assessment of creep strength of welded joints. The lifetime of the welded structure is primarily determined by the behavior in the local zones of welds, where time-dependent creep and damage processes dominate. Different types of creep failure that have occurred in recent years are discussed in [29], for example. The design of welded structures and their residual-life estimations require engineering mechanics models that would be able to characterize creep strains, stress redistributions, and damage evolution in the zones of welds.

A weld is usually considered as a metallurgical notch. The reason for this is the complex microstructure in the weld metal itself and in the neighboring heat-affected zone. In recent years many research activities have been directed to the study of welded joints. First, theoretical and experimental analyses have addressed the welding process with the aim of predicting the formation of the microstructure of the welds and analyzing residual stresses [7]. Second, the behavior of welded joints under mechanical and thermal loadings was investigated [21]. Here one must consider that the stress–strain response at room temperature is quite different for the weld metal, the heat-affected zone, and the base metal (parent material), particularly if they are loaded beyond the yield limit. At elevated temperatures quite different inelastic strain versus time curves

K. Naumenko (✉) · H. Altenbach
Martin-Luther-University Halle-Wittenberg, Department of Engineering Sciences, 06099 Halle, Germany
E-mail: konstantin.naumenko@iw.uni-halle.de

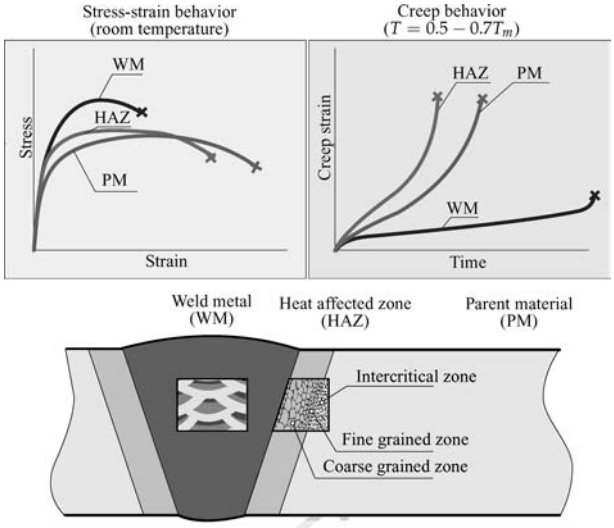

Fig. 1 Typical microstructure of a welded joint and material behavior

can be obtained in different zones even in the case of a constant moderate load. Figure 1 illustrates zones with different microstructures and the variation in material behavior within the weld.

The results of creep testing of cross-weld specimens [19,20] and specimens with a simulated microstructure [24,25,30,31] show significant variation in creep properties in different material zones within the weld. Furthermore, they illustrate that the intercritical region of the heat-affected zone is the weakest part of the weld with respect to creep properties. The material with the heat-affected zone microstructure usually exhibits the highest creep rate and the shortest time to failure compared to other material zones within the weld for the same load and temperature.

For thick and moderately thick cross sections multipass welding is usually preferred, where many stringer beads are deposited in a defined sequence. As a result of heating and cooling cycles during the welding process, a complex bead-type microstructure of the weld metal is formed, where every single bead consists of columnar, coarse-grained, and fine-grained regions, e.g., [21]. The results of uniaxial creep tests for the weld metal 9CrMoNbV are reported in [18]. They show that the creep strain versus time curves differ significantly for specimens removed from the weld metal in the longitudinal (welding) direction and the transverse direction. Furthermore, different types of damage were observed for the longitudinal and the transverse specimens.

One possibility for studying the creep behavior in structures is the use of continuum damage mechanics, e.g., [3,4,16]. The application of this approach to welded joints is discussed in [15,17,21], for example. Here the weld is considered a heterogeneous structure composed of at least three constituents—the weld metal, the heat-affected zone, and the parent material—with different creep properties. Constitutive and evolution equations that are able to reflect experimental data of primary, secondary, and tertiary creep in different zones of the welded joint are presented in [14,15,17,21,30], among others. The results of finite-element simulations illustrate stress redistributions, creep strains, and damage evolution in different zones of the weld [14,15,17, 21]. Furthermore, they allow one to analyze the influence of numerous factors such as weld dimensions, types of external loading, and material properties on the creep behavior of welded structures, e.g., [21]. However, as far as we know, the anisotropic creep of multipass weld metals has not been considered.

The objective of this paper is the phenomenological modeling of the anisotropic creep behavior of a multipass weld metal. To explain the origins of anisotropic creep, we introduce first a uniaxial model for a binary structure composed of fine-grained and coarse-grained constituents with different creep properties. This model illustrates the basic features of the stress redistribution and damage growth in the constituents of the weld metal. The structural analysis of a welded joint would require a model of creep for the weld metal under multiaxial stress states. For this purpose we apply the engineering creep theory, which is based on the creep potential hypothesis, the flow rule, and internal state variables, e.g., [9]. The response functions and the material constants are identified for the experimental data presented in [18].

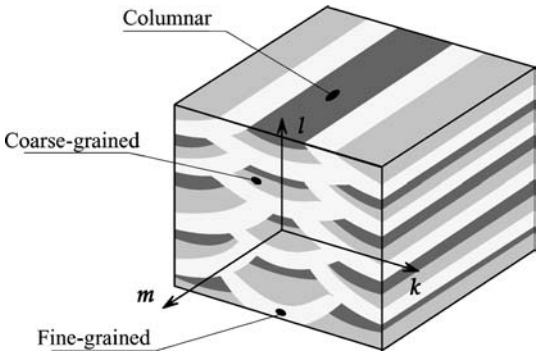

Fig. 2 Microstructure of the weld metal (after [21])

2 Origins of anisotropic creep

A weld bead produced by a single-pass welding has a columnar solidification microstructure. During multipass welding many weld beads are deposited in the groove according to a defined sequence. As a subsequent weld bead is laid, the part of the metal produced in previous cycles is subjected to local reheating and cooling. As a result, the weld beads consist of columnar, coarse-grained, and fine-grained microstructural zones [18,21]. A sketch of the typical microstructure of a multipass weld metal is presented in Fig. 2. This microstructure depends on many factors of the welding process, such as bead size, travel speed, build-up sequence, interpass temperature, and type of postweld heat treatment [18]. The resulting inelastic material behavior will be apparently determined by the distribution and size of columnar, coarse-grained, and fine-grained zones as well as residual stresses in the weld metal. It is well established that creep behavior is very sensitive to the type of microstructure and, in particular, to the grain size. Experimental data illustrating the significant influence of grain size on creep behavior are presented for copper in [22] and for various types of steel in [24,30,31]. The grain-size dependence is explained in materials science by two creep mechanisms: grain boundary sliding and grain boundary diffusion. These mechanisms operate under moderate loading and within a temperature range of $0.5 < T/T_m < 0.7$, where T_m is the melting temperature, e.g., [26]. The principal damage mechanism is the nucleation and growth of voids on grain boundaries. Many experimental observations show that the finer the grain structure, the higher the secondary creep rate and the higher the damage rate for the same loading and temperature conditions.

To discuss the origins of the anisotropic creep in a weld metal let us consider a uniaxial model of a binary structure composed of constituents with different creep properties. In what follows let us term the first constituent fine-grained or creep-weak and the second one coarse-grained or creep-strong. Let us describe the creep behavior of constituents by use of the Kachanov–Rabotnov model (e.g., [23]):

$$\dot{\varepsilon}^{\mathrm{cr}} = \frac{a\sigma^n}{(1-\omega)^n}, \qquad \dot{\omega} = \frac{b\sigma^k}{(1-\omega)^l}\,. \tag{2.1}$$

Here $\varepsilon^{\mathrm{cr}}$ is the creep strain; σ is the stress; $0 \le \omega < 1$ is the phenomenological damage parameter; a, b, n, k, and l are material constants; and the dot denotes the time derivative. Equations (2.1) ignore the primary creep and describe only the secondary and tertiary creep stages. For $\omega = 0$ the minimum creep rate equation $\dot{\varepsilon}^{\mathrm{cr}}_{\mathrm{min}} = a\sigma^n$ follows from (2.1). The material constants a and n are usually determined from experimental data for minimum creep rate versus stress. The time integration of (2.1) provides

$$t_* = \frac{1}{(l+1)b\sigma^k}, \qquad \varepsilon^{\mathrm{cr}}_* = \frac{a\sigma^{n-k}}{b(l+1-n)}\,, \tag{2.2}$$

where t_* is the time to fracture and $\varepsilon^{\mathrm{cr}}_*$ is the fracture strain. The material constants b, k, and l can be determined from the long-term strength diagram, i.e., the time to fracture versus stress dependence, as well as from the fracture strain versus stress dependence. In what follows we use the subscripts f and c for the fine-grained and coarse-grained constituents, respectively. For the sake of simplicity we assume that the constituents have the same value of Young's modulus E and the same values of constants n, k, and l in (2.1). Let us introduce

the dimensionless quantities

$$s = \frac{\sigma}{\sigma_0}, \quad \epsilon = \frac{\varepsilon}{\varepsilon_0}, \quad \epsilon^{\rm cr} = \frac{\varepsilon^{\rm cr}}{\varepsilon_0}, \quad \tau = \frac{t}{t_{*_f}}, \tag{2.3}$$

where t_{*_f} is the time to fracture of the fine-grained constituent, σ_0 is the reference stress, and ε_0 is the elastic strain at σ_0, i.e., $\varepsilon_0 = \sigma_0/E$. Equations (2.1) can be formulated for two constituents as follows:

$$\left\{ \begin{array}{l} \dfrac{{\rm d}\epsilon_f^{\rm cr}}{{\rm d}\tau} = \tilde{a}\dfrac{s^n}{(1-\omega_f)^n} \\ \dfrac{{\rm d}\omega_f}{{\rm d}\tau} = \tilde{b}\dfrac{s^k}{(1-\omega_f)^l} \end{array} \right. , \quad \left\{ \begin{array}{l} \dfrac{{\rm d}\epsilon_c^{\rm cr}}{{\rm d}\tau} = \alpha\tilde{a}\dfrac{s^n}{(1-\omega_c)^n} \\ \dfrac{{\rm d}\omega_c}{{\rm d}\tau} = \beta\tilde{b}\dfrac{s^k}{(1-\omega_c)^l} \end{array} \right. , \tag{2.4}$$

where

$$\tilde{a} = \epsilon_{*_f}\left(1 - \frac{n}{l+1}\right), \quad \tilde{b} = \frac{1}{l+1}, \quad \alpha = \frac{\dot{\varepsilon}^{\rm cr}_{\min_c}}{\dot{\varepsilon}^{\rm cr}_{\min_f}}, \quad \beta = \frac{t_{*_f}}{t_{*_c}}.$$

Figure 3 illustrates creep curves obtained after integration of (2.4) for the cases $n = 3$, $k = n+1$, $l = n+2$, $\epsilon_{*_f} = 5$, $\alpha = 0.15$, $\beta = 0.25$, and $s = 1$.

Let us consider a connection of constituents in parallel, as is usually the case for composite materials, e.g., [1,12]. In this case the strains and the strain rates can be assumed to be the same (isostrain concept):

$$\varepsilon \equiv \varepsilon_f = \varepsilon_c, \quad \dot{\varepsilon} \equiv \dot{\varepsilon}_f = \dot{\varepsilon}_c. \tag{2.5}$$

We assume that a constant load $F = \sigma_0 A$, Fig. 4, is applied to the binary structure, where A is the cross-sectional area.

Specifying by N_f and N_c the internal forces in constituents so that $N_f + N_c = F$, we can write

$$\sigma_f A_f + \sigma_c A_c = \sigma_0 A, \quad \eta_f\sigma_f + (1-\eta_f)\sigma_c = \sigma_0, \quad \eta_f s_f + (1-\eta_f)s_c = 1, \tag{2.6}$$

where $\eta_f = A_f/A$ is the volume fraction of the fine-grained constituent. For the stresses we apply the following constitutive equations

$$\sigma_f = E(\varepsilon - \varepsilon_f^{\rm cr}), \quad \sigma_c = E(\varepsilon - \varepsilon_c^{\rm cr}). \tag{2.7}$$

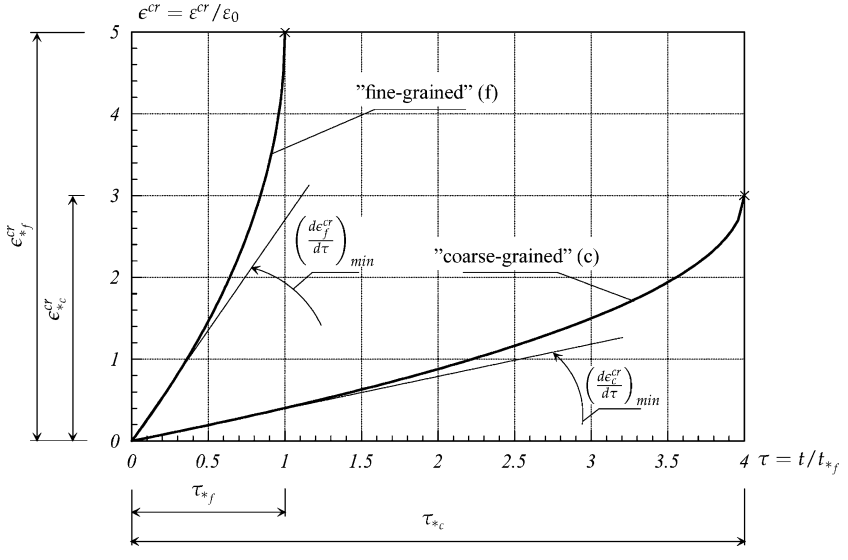

Fig. 3 Creep curves for constituents

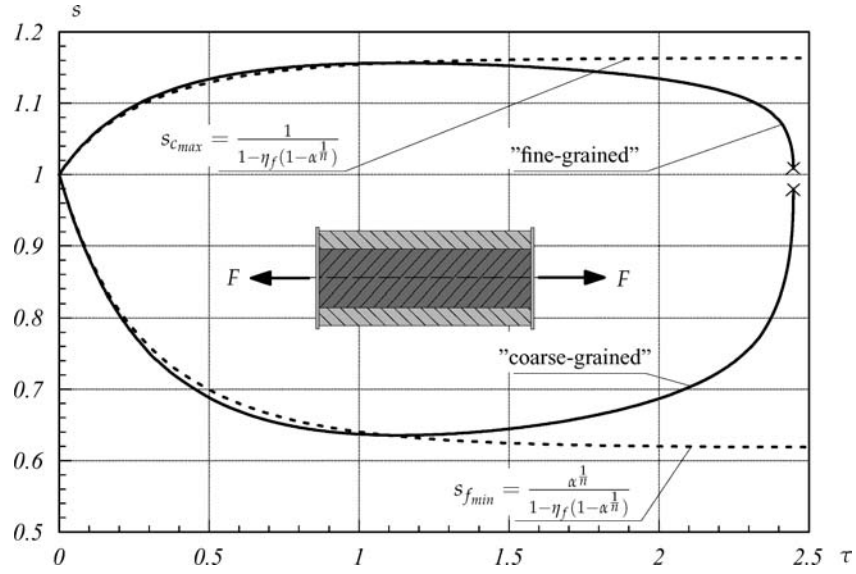

Fig. 4 Normalized stresses versus normalized time for connection of constituents in parallel

Based on (2.4)–(2.7) one can formulate a system of ordinary differential equations describing the stress redistribution between constituents. With respect to the stress in the fine-grained constituent, the following equation can be obtained:

$$\frac{\mathrm{d}s_f}{\mathrm{d}\tau} = \bar{a}(1-\eta_f)\left[\frac{\alpha}{(1-\eta_f)^n}\frac{(1-\eta_f s_f)^n}{(1-\omega_c)^n} - \frac{s_f^n}{(1-\omega_f)^n}\right]. \tag{2.8}$$

Equation (2.8) is numerically solved together with the evolution equations for damage parameters (2.4) and initial conditions $s_f = 1$, $\omega_f = \omega_c = 0$ providing the time variation of the stress s_f. The stress s_c can then be computed from (2.6). The results are shown in Fig. 4 for the case $\eta_f = 0.3$. In addition, Fig. 5 presents creep strains and the damage parameters in constituents as well as the creep strain of the composite $\epsilon^{\mathrm{cr}} \equiv \epsilon - 1$. At the beginning of the creep process the creep rate is higher in the fine-grained constituent, Fig. 5a. Therefore, the stress in the fine-grained constituent relaxes while the stress in the coarse-grained constituent increases, Fig. 4. If we neglect the influence of damage on the creep process, i.e., set $\omega_f = \omega_c = 0$ in (2.8), we obtain the steady-state creep solution. The corresponding results are plotted in Fig. 4 by dotted lines. We observe that the maximum value of s_c and the minimum value of s_f in the case of creep damage almost coincide with the corresponding steady-state values. The steady-state solution for s_f follows from (2.8) by setting $\omega_f = \omega_c = 0$

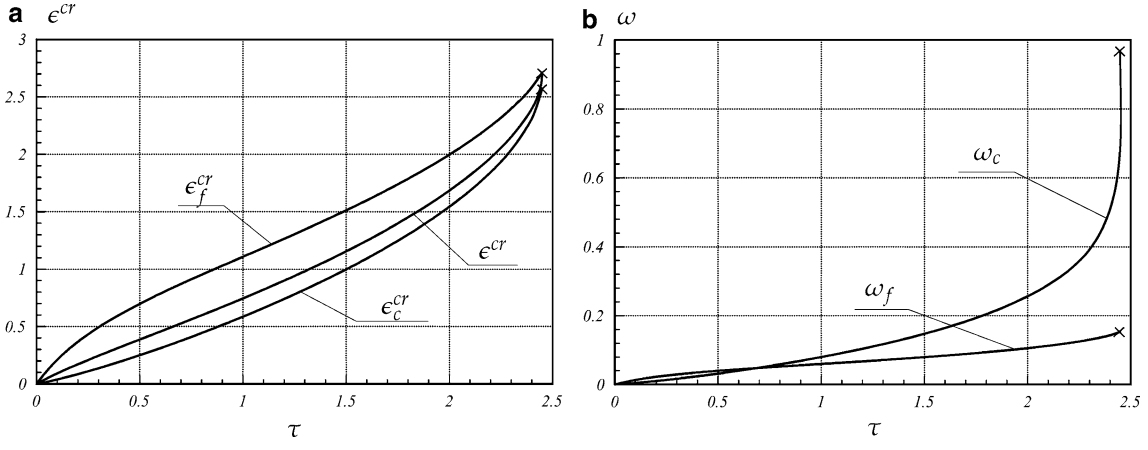

Fig. 5 Connection of constituents in parallel. **a** Normalized creep strains versus normalized time. **b** Damage parameters versus normalized time

and $\mathrm{d}s_f/\mathrm{d}\tau = 0$. The corresponding value for s_c is obtained from (2.6). The results are

$$s_{f_{\min}} = \frac{\alpha^{\frac{1}{n}}}{1-\eta_f(1-\alpha^{\frac{1}{n}})}, \quad s_{c_{\max}} = \frac{1}{1-\eta_f(1-\alpha^{\frac{1}{n}})}.$$

We observe that these stress values are determined by the volume fraction of the fine-grained constituent η_f and the ratio of minimum creep rates α. The stress value s_c is higher than s_f after the initial stress redistribution. Therefore, the coarse-grained constituent exhibits the higher creep rate and the higher damage rate in the final stage of the creep process, Fig. 5. The calculation predicts the failure initiation in the coarse-grained constituent.

In the case of a connection of constituents in series (isostress approach) we assume

$$\sigma_0 = \sigma_f = \sigma_c, \quad \varepsilon^{\mathrm{cr}} = \eta_f \varepsilon_f^{\mathrm{cr}} + (1-\eta_f)\varepsilon_c^{\mathrm{cr}}.$$

The results can be obtained by integration (2.4) for $s_f = s_c = 1$. The corresponding plots of normalized creep strains are presented in Fig. 3. The maximum creep and damage rates are now in the fine-grained constituent. The lifetime of the binary structure is determined by the lifetime of the fine-grained constituent for the given constant stress.

Figure 6 shows the creep curves obtained for the two considered cases of the binary structure under the same constant load. The results of the presented model provide an analogy to the creep behavior of a weld metal loaded in the longitudinal (welding) and transverse directions. The experimental creep curves for the specimen removed from the weld metal in two directions are presented in [18]. They show that the transverse specimens exhibit higher minimum creep rate. Furthermore, the creep curves for transverse specimens have a much shorter tertiary stage and lower values of fracture strain compared to curves for specimens removed in the welding direction. The times to rupture for the transverse specimens are much shorter than those for the longitudinal specimens. From the results in Fig. 6 we observe that these effects are predicted by the mechanical model of the binary structure. Furthermore, our results for the damage evolution qualitatively agree with the results of microstructural damage observations presented in [18]. For the longitudinal specimens extensive voids and cracks were observed in columnar and coarse-grained regions along the entire specimen length. For the transverse specimen voids and cracks are localized near the fracture surface. The fracture surface has fine-grained structure and the failure propagated through the fine-grained regions of the specimens.

Based on the presented results we may conclude that of the many different creep and damage mechanisms that may operate and interact during the creep process an essential role is played by the stress redistribution between the creep-weak and creep-strong constituents. For longitudinal specimens this mechanism leads to a prolonged tertiary creep stage. The material behaves like a more ductile material, although the damage and failure occur in the more-brittle creep-strong constituent.

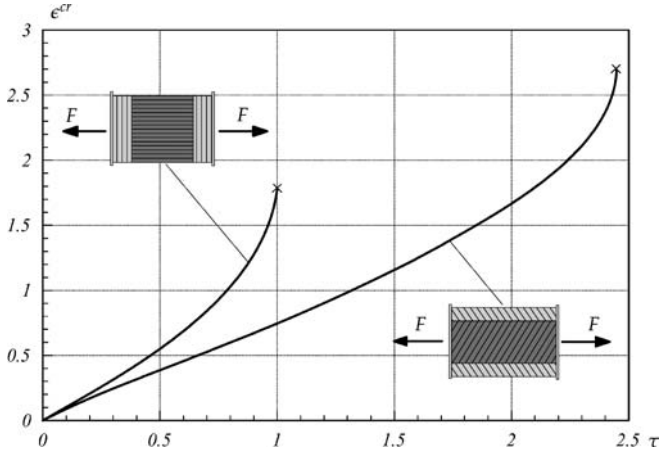

Fig. 6 Creep curves for the binary structure in the cases of parallel and series connections of the constituents

3 Secondary creep under multiaxial stress states

For the analysis of welded structures, a model that is able to reflect anisotropic creep in a weld metal under multiaxial stress states must be developed. Three-dimensional models for binary or multicomponent media are discussed within the framework of continuum mechanics (e.g., [6]). A generalization of the composite model developed in the previous section to the multiaxial stress states would, however, require the knowledge of creep properties of constituents under multiaxial stress states. Furthermore, creep mechanisms of interaction between constituents, like frictional sliding, should be taken into account.

In what follows we assume the weld metal to be a quasihomogeneous anisotropic material. For a description of creep we prefer the engineering creep mechanics approach, where the creep potential hypothesis, the representation of tensor functions, and internal state variables, e.g., [9], are incorporated. The resulting constitutive equations are compatible with the finite-element method and can be used in standard finite-element codes for structural analysis purposes.

Examples of anisotropic creep behavior and related constitutive equations are presented for single-crystal alloys in [8] and for fiber-reinforced materials in [28]. One problem of anisotropic creep modeling is that the assumed material symmetries (microstructure symmetries) are difficult to verify in creep tests due to the relatively large scatter of experimental data. Furthermore, the material may lose some or even all symmetries during the creep as a consequence of hardening and damage processes. In our case the material symmetries can be established according to the arrangement of the weld beads in the weld metal. For the structure presented in Fig. 2 one can assume the reflection $\boldsymbol{Q}_1 = \boldsymbol{I} - 2\boldsymbol{m} \otimes \boldsymbol{m}$, the rotation $\boldsymbol{Q}_2 = 2\boldsymbol{l} \otimes \boldsymbol{l} - \boldsymbol{I}$, and the reflection $\boldsymbol{Q}_3 = \boldsymbol{Q}_1 \cdot \boldsymbol{Q}_2 = \boldsymbol{I} - 2\boldsymbol{k} \otimes \boldsymbol{k}$ to be the elements of the material symmetry group, where $\boldsymbol{I}$ is the second rank unit tensor and $\boldsymbol{k}, \boldsymbol{l}$, and $\boldsymbol{m}$ are orthogonal unit vectors.

However, this material symmetry group is poor for the modeling of creep. Indeed, based on the model discussed in the previous section, we can assume that the same creep mechanisms will operate by loading the weld metal in the $\boldsymbol{k}$- or $\boldsymbol{l}$-directions. Although the experimental data presented in [18] are available only for specimens removed in the $\boldsymbol{m}$- and $\boldsymbol{k}$-directions, one may assume that the difference between experimental creep curves by loading in the $\boldsymbol{k}$- and $\boldsymbol{l}$-directions will be nonessential with respect to the usual scatter of experimental data. Here we assume transversely isotropic creep, where the plane spanned on the vectors $\boldsymbol{k}$ and $\boldsymbol{l}$ is the quasi-isotropy plane.

Following the creep theory proposed by Odqvist [27], the creep rate tensor $\dot{\boldsymbol{\varepsilon}}^{cr}$ is defined by the creep potential W and the flow rule

$$\dot{\boldsymbol{\varepsilon}}^{cr} = \frac{\partial W}{\partial \boldsymbol{\sigma}}, \quad W = W(\boldsymbol{\sigma}, T), \tag{3.1}$$

where $\boldsymbol{\sigma}$ is the Cauchy stress tensor and T is the absolute temperature. In what follows, the dependence on the temperature will be dropped for the sake of brevity. According to the assumed symmetries, the creep potential must satisfy the following restriction:

$$W\left(\boldsymbol{Q}(\varphi\boldsymbol{m}) \cdot \boldsymbol{\sigma} \cdot \boldsymbol{Q}^{\mathrm{T}}(\varphi\boldsymbol{m})\right) = W(\boldsymbol{\sigma}), \quad Q(\varphi\boldsymbol{m}) = \boldsymbol{m} \otimes \boldsymbol{m} + \cos\,\varphi(\boldsymbol{I} - \boldsymbol{m} \otimes \boldsymbol{m}) + \sin\,\varphi\boldsymbol{m} \times \boldsymbol{I}. \tag{3.2}$$

In (3.2) $Q(\varphi\boldsymbol{m})$ is the assumed symmetry transformation, where $\boldsymbol{m}$ is the constant unit vector and φ is the arbitrary angle of rotation about $\boldsymbol{m}$. Taking the derivative of the first equation (3.2) with respect to φ we obtain

$$\frac{\mathrm{d}W}{\mathrm{d}\varphi} = \frac{\mathrm{d}\boldsymbol{\sigma}'}{\mathrm{d}\varphi} \cdot\cdot \left(\frac{\partial W}{\partial \boldsymbol{\sigma}'}\right)^{\mathrm{T}} = 0, \quad \boldsymbol{\sigma}' \equiv \boldsymbol{Q}(\varphi\boldsymbol{m}) \cdot \boldsymbol{\sigma} \cdot \boldsymbol{Q}^{\mathrm{T}}(\varphi\boldsymbol{m}). \tag{3.3}$$

The derivative of $\boldsymbol{\sigma}'$ with respect to φ can be calculated by the following rules:

$$\begin{aligned} &\mathrm{d}\boldsymbol{\sigma}'(\varphi) = \mathrm{d}\boldsymbol{Q}(\varphi\boldsymbol{m}) \cdot \boldsymbol{\sigma} \cdot \boldsymbol{Q}^{\mathrm{T}}(\varphi\boldsymbol{m}) + \boldsymbol{Q}(\varphi\boldsymbol{m}) \cdot \boldsymbol{\sigma} \cdot d\boldsymbol{Q}^{\mathrm{T}}(\varphi\boldsymbol{m}), \\ &\mathrm{d}\boldsymbol{Q}(\varphi\boldsymbol{m}) = \boldsymbol{m} \times \boldsymbol{Q}(\varphi\boldsymbol{m})\mathrm{d}\varphi \quad \Rightarrow \quad \mathrm{d}\boldsymbol{Q}^{\mathrm{T}}(\varphi\boldsymbol{m}) = -\boldsymbol{Q}^{\mathrm{T}}(\varphi\boldsymbol{m}) \times \boldsymbol{m}d\varphi. \end{aligned} \tag{3.4}$$

By inserting (3.4) into (3.3) the following partial differential equation can be obtained:

$$(\boldsymbol{m} \times \boldsymbol{\sigma} - \boldsymbol{\sigma} \times \boldsymbol{m}) \cdot\cdot \left(\frac{\partial W}{\partial \boldsymbol{\sigma}}\right)^{\mathrm{T}} = 0. \tag{3.5}$$

The set of integrals of this equation is the set of functionally independent scalar-valued arguments of the potential W. They represent the invariants of $\boldsymbol{\sigma}$ with respect to the assumed symmetry transformation. The characteristic system of (3.5) is the system of ordinary differential equations

$$\frac{\mathrm{d}\boldsymbol{\sigma}}{\mathrm{d}s} = (\boldsymbol{m} \times \boldsymbol{\sigma} - \boldsymbol{\sigma} \times \boldsymbol{m}). \tag{3.6}$$

Any system of n linear ordinary differential equations has no more than $n-1$ functionally independent integrals [13]. Since $\boldsymbol{\sigma}$ is symmetric, (3.6) is the system of six ordinary differential equations and has no more than five functionally independent integrals. One may prove that the integrals of (3.6) are [5]

$$I_k = \mathrm{tr}\,(\boldsymbol{\sigma}^k), \quad k = 1, 2, 3, \quad I_4 = \boldsymbol{m} \cdot \boldsymbol{\sigma} \cdot \boldsymbol{m}, \quad I_5 = \boldsymbol{m} \cdot \boldsymbol{\sigma}^2 \cdot \boldsymbol{m}, \quad I_6 = \boldsymbol{m} \cdot \boldsymbol{\sigma}^2 \cdot (\boldsymbol{m} \times \boldsymbol{\sigma} \cdot \boldsymbol{m}). \tag{3.7}$$

The invariants with respect to different symmetry transformations are discussed in [11] (see also relevant references therein). For the case of the transverse isotropy, the authors derived six invariants applying another approach. In this sense our result coincides with the result given in [11]. However, from our approach it follows that only five invariants listed in (3.7) are functionally independent. The relation between the invariants can be formulated as follows [5]:

$$\mathrm{I}_6^2 = \det \begin{pmatrix} 1 & \mathrm{I}_4 & \mathrm{I}_5 \\ \mathrm{I}_4 & \mathrm{I}_5 & \boldsymbol{m} \cdot \boldsymbol{\sigma}^3 \cdot \boldsymbol{m} \\ \mathrm{I}_5 & \boldsymbol{m} \cdot \boldsymbol{\sigma}^3 \cdot \boldsymbol{m} & \boldsymbol{m} \cdot \boldsymbol{\sigma}^4 \cdot \boldsymbol{m} \end{pmatrix}. \tag{3.8}$$

It can be verified that $\boldsymbol{m} \cdot \boldsymbol{\sigma}^3 \cdot \boldsymbol{m}$ and $\boldsymbol{m} \cdot \boldsymbol{\sigma}^4 \cdot \boldsymbol{m}$ are transversely isotropic invariants too. However, applying the Cayley–Hamilton theorem, e.g., [9], they can be expressed by $I_1, I_2, \ldots, I_5$.

Assuming that the rotation $\boldsymbol{Q}(\pi \boldsymbol{l}) = 2\boldsymbol{l} \otimes \boldsymbol{l} - \boldsymbol{I}, \boldsymbol{l} \cdot \boldsymbol{m} = 0$ belongs to the symmetry group of the transverse isotropy, the last invariant I_6 can be omitted [5] and $W(\boldsymbol{\sigma}) = W(I_1, I_2, I_3, I_4, I_5)$. The invariants $I_1, I_2, \ldots, I_5$ are widely used in constitutive equations for transversely isotropic media, e.g., [9,10,28]. In what follows we prefer another set of invariants that can be related to (3.7) and has a clearer mechanical interpretation. Let us decompose the stress tensor as follows:

$$\boldsymbol{\sigma} = a_m \boldsymbol{m} \otimes \boldsymbol{m} + \boldsymbol{\sigma}_p + \boldsymbol{\tau}_m \otimes \boldsymbol{m} + \boldsymbol{m} \otimes \boldsymbol{\tau}_m \tag{3.9}$$

with the projections

$$a_m = \boldsymbol{m} \cdot \boldsymbol{\sigma} \cdot \boldsymbol{m}, \quad \boldsymbol{\sigma}_p = (\boldsymbol{I} - \boldsymbol{m} \otimes \boldsymbol{m}) \cdot \boldsymbol{\sigma} \cdot (\boldsymbol{I} - \boldsymbol{m} \otimes \boldsymbol{m}), \quad \boldsymbol{\tau}_m = \boldsymbol{m} \cdot \boldsymbol{\sigma} \cdot (\boldsymbol{I} - \boldsymbol{m} \otimes \boldsymbol{m}). \tag{3.10}$$

In (3.9) a_m is the normal stress acting in the plane with the unit normal $\boldsymbol{m}$, and $\boldsymbol{\sigma}_p$ stands for the plane part of the stress tensor representing the stress state in the isotropy plane. $\boldsymbol{\tau}_m$ is the transverse shear stress vector in the plane with the unit normal $\boldsymbol{m}$. For the orthonormal basis $\boldsymbol{k}, \boldsymbol{l}$, and $\boldsymbol{m}$ the projections are (Fig. 7)

$$\sigma_{mm} = a_m, \quad \boldsymbol{\tau}_m = \tau_{mk}\boldsymbol{k} + \tau_{ml}\boldsymbol{l}, \quad \boldsymbol{\sigma}_p = \sigma_{kk}\boldsymbol{k} \otimes \boldsymbol{k} + \sigma_{ll}\boldsymbol{l} \otimes \boldsymbol{l} + \tau_{kl}(\boldsymbol{k} \otimes \boldsymbol{l} + \boldsymbol{l} \otimes \boldsymbol{k}).$$

The plane part of the stress tensor can be further decomposed as follows:

$$\boldsymbol{\sigma}_p = \boldsymbol{s}_p + a_p(\boldsymbol{I} - \boldsymbol{m} \otimes \boldsymbol{m}), \quad \mathrm{tr}\,\boldsymbol{s}_p = 0 \quad \Rightarrow \quad a_p = \frac{1}{2}\mathrm{tr}\,\boldsymbol{\sigma}_p. \tag{3.11}$$

Now instead of (3.7) we can introduce the following set of transversely isotropic invariants:

$$\begin{aligned} &I_{1m} = \boldsymbol{m} \cdot \boldsymbol{\sigma} \cdot \boldsymbol{m}, \quad && I_{2m} = \mathrm{tr}\,\boldsymbol{\sigma}_p, && I_{3m} = \frac{1}{2}\mathrm{tr}\,\boldsymbol{s}_p^2, \\ &I_{4m} = \boldsymbol{\tau_m} \cdot \boldsymbol{\tau_m}, && I_{5m} = \boldsymbol{\tau_m} \cdot \boldsymbol{s}_p \cdot \boldsymbol{\tau_m}, && I_{6m} = \boldsymbol{m} \cdot (\boldsymbol{\tau_m} \cdot \boldsymbol{s}_p \times \boldsymbol{\tau_m}). \end{aligned} \tag{3.12}$$

It is shown in [5] that the invariants above are integrals of (3.5). Only five of them are functionally independent due to the relation $I_{6m}^2 = I_{3m} I_{4m}^2 - I_{5m}^2$. In what follows we assume $\boldsymbol{Q}(\pi \boldsymbol{l})$ to be the additional symmetry transformation. In this case I_{6m} can be omitted [5].

I_{5m} is the cubic invariant. Cubic invariants of the stress tensor are considered to describe nonclassical and second-order effects like different creep rates by tension and compression or elongation rate under shear

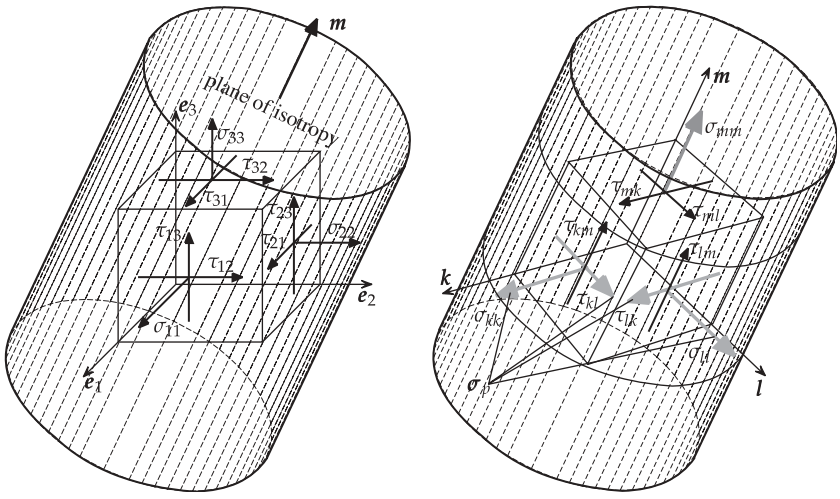

Fig. 7 Stress state in a transversely isotropic medium and corresponding projections σ_{mm}, $\boldsymbol{\sigma}_p$, and $\boldsymbol{\tau}_m$

stress [2,9]. Here we neglect such effects. The creep potential is then a function of four arguments, i.e., $W(\boldsymbol{\sigma}) = W(I_{1m}, I_{2m}, I_{3m}, I_{4m})$. The flow rule (3.1) results in the following creep equation:

$$\dot{\boldsymbol{\varepsilon}}^{\mathrm{cr}} = \frac{\partial W}{\partial I_{1m}}\boldsymbol{m}\otimes\boldsymbol{m} + \frac{\partial W}{\partial I_{2m}}(\boldsymbol{I} - \boldsymbol{m}\otimes\boldsymbol{m}) + \frac{\partial W}{\partial I_{3m}}\boldsymbol{s}_p + \frac{\partial W}{\partial I_{4m}}(\boldsymbol{\tau}_{\boldsymbol{m}}\otimes\boldsymbol{m} + \boldsymbol{m}\otimes\boldsymbol{\tau}_{\boldsymbol{m}}). \tag{3.13}$$

The next assumption usually employed in the creep theory is the zero volumetric creep rate [27]. Setting the trace of (3.13) to zero we obtain

$$\mathrm{tr}\,\dot{\boldsymbol{\varepsilon}}^{\mathrm{cr}} = \frac{\partial W}{\partial I_{1m}} + 2\frac{\partial W}{\partial I_{2m}} = 0 \quad \Rightarrow \quad W = W\left(I_{1m} - \frac{1}{2}I_{2m}, I_{3m}, I_{4m}\right). \tag{3.14}$$

Introducing the notation $J_m \equiv I_{1m} - \frac{1}{2}I_{2m}$ the creep equation (3.13) takes the form

$$\dot{\boldsymbol{\varepsilon}}^{cr} = \frac{1}{2}\frac{\partial W}{\partial J_m}(3\boldsymbol{m}\otimes\boldsymbol{m} - \boldsymbol{I}) + \frac{\partial W}{\partial I_{3m}}\boldsymbol{s}_p + \frac{\partial W}{\partial I_{4m}}(\boldsymbol{\tau}_{\boldsymbol{m}}\otimes\boldsymbol{m} + \boldsymbol{m}\otimes\boldsymbol{\tau}_{\boldsymbol{m}}). \tag{3.15}$$

By analogy to the case of isotropic creep [27] we introduce the equivalent stress as follows:

$$\sigma_{\mathrm{eq}}^2 = \alpha_1 J_m^2 + 3\alpha_2 I_{3m} + 3\alpha_3 I_{4m} = \alpha_1\left(\boldsymbol{m}\cdot\boldsymbol{\sigma}\cdot\boldsymbol{m} - \frac{1}{2}\mathrm{tr}\,\boldsymbol{\sigma}_p\right)^2 + \frac{3}{2}\alpha_2\mathrm{tr}\,\boldsymbol{s}_p^2 + 3\alpha_3\tau_{\boldsymbol{m}}^2. \tag{3.16}$$

The positive definiteness of the quadratic form (3.16) is provided by the conditions $\alpha_i > 0$, $i = 1, 2, 3$. With the equivalent stress (3.16) the final form of the creep equation is

$$\dot{\boldsymbol{\varepsilon}}^{\mathrm{cr}} = \frac{3}{2}\frac{\dot{\varepsilon}_{\mathrm{eq}}}{\sigma_{\mathrm{eq}}}\left[\alpha_1 J_m\left(\boldsymbol{m}\otimes\boldsymbol{m} - \frac{1}{3}\boldsymbol{I}\right) + \alpha_2\boldsymbol{s}_p + \alpha_3(\boldsymbol{\tau}_m\otimes\boldsymbol{m} + \boldsymbol{m}\otimes\boldsymbol{\tau}_m)\right], \quad \dot{\varepsilon}_{\mathrm{eq}} \equiv \frac{\partial W}{\partial\sigma_{\mathrm{eq}}}. \tag{3.17}$$

The advantage of the introduced invariants (3.12) over (3.7) is that they can be specified independently of each other. For example, set the second invariant in (3.7) equal to zero, i.e., $\mathrm{tr}\,\boldsymbol{\sigma}^2 = \boldsymbol{\sigma}\cdot\cdot\,\boldsymbol{\sigma} = 0$. From this it follows that $\boldsymbol{\sigma} = \boldsymbol{0}$ and consequently all other invariants listed in (3.7) are simultaneously equal to zero. In addition, the introduced invariants can be related to typical stress states that should be realized in creep tests for the identification of constitutive functions and material constants.

The deviatoric part $\boldsymbol{s}$ of the stress tensor and its second principal invariant are computed by

$$\boldsymbol{s} = J_m\left(\boldsymbol{m}\otimes\boldsymbol{m} - \frac{1}{3}\boldsymbol{I}\right) + \boldsymbol{s}_p + \boldsymbol{\tau}_m\otimes\boldsymbol{m} + \boldsymbol{m}\otimes\boldsymbol{\tau}_m, \quad \mathrm{tr}\,\boldsymbol{s}^2 = \frac{2}{3}J_m^2 + \mathrm{tr}\,\boldsymbol{s}_p^2 + 2\tau_{\boldsymbol{m}}^2. \tag{3.18}$$

Setting in (3.16) and (3.17) $\alpha_1 = \alpha_2 = \alpha_3 = 1$ and taking into account (3.18) we obtain the Norton–Bailey–Odqvist constitutive equation for isotropic secondary creep [27]:

$$\dot{\boldsymbol{\varepsilon}}^{\mathrm{cr}} = \frac{3}{2}\frac{\dot{\varepsilon}_{\mathrm{eq}}}{\sigma_{vM}}\boldsymbol{s}, \quad \sigma_{vM}^2 = \frac{3}{2}\mathrm{tr}\,\boldsymbol{s}^2,$$

where σ_{vM} is the von Mises equivalent stress.

4 Identification of material constants and constitutive functions

In the equivalent stress expression (3.16) α_i plays the role of dimensionless factors. Three independent uniform stress states should be realized in order to determine α_i. The relevant stress states are

– Uniaxial tension in the direction $\boldsymbol{m}$ (longitudinal tension test). In this case $\boldsymbol{\sigma} = \sigma_0 \boldsymbol{m} \otimes \boldsymbol{m}$, where $\sigma_0 > 0$ is the magnitude of the applied stress. From (3.16) and (3.17) it follows that

$$J_m = \sigma_0, \quad I_{3m} = I_{4m} = 0, \quad \sigma_{\mathrm{eq}} = \sigma_0\sqrt{\alpha_1}, \quad \dot{\boldsymbol{\varepsilon}}^{cr} = \sqrt{\alpha_1}\dot{\varepsilon}_{\mathrm{eq}}\left[\boldsymbol{m}\otimes\boldsymbol{m} - \frac{1}{2}(\boldsymbol{I} - \boldsymbol{m}\otimes\boldsymbol{m})\right]. \quad (4.1)$$

– Uniaxial tension in the direction $\boldsymbol{k}$ (transverse tension test), i.e., $\boldsymbol{\sigma} = \sigma_0 \boldsymbol{k}\otimes\boldsymbol{k}$, $\sigma_0 > 0$. From (3.16) and (3.17) we obtain

$$\begin{aligned} &\boldsymbol{s}_p = \frac{1}{2}\sigma_0(\boldsymbol{k}\otimes\boldsymbol{k} - \boldsymbol{l}\otimes\boldsymbol{l}), \quad J_m = -\frac{1}{2}\sigma_0, \quad I_{3m} = \frac{1}{4}\sigma_0^2, \quad I_{4m} = 0, \quad \sigma_{\mathrm{eq}} = \frac{1}{2}\sigma_0\sqrt{\alpha_1 + 3\alpha_2}, \\ &\dot{\boldsymbol{\varepsilon}}^{cr} = \frac{\dot{\varepsilon}_{\mathrm{eq}}}{2\sqrt{\alpha_1 + 3\alpha_2}}\left[(\alpha_1 + 3\alpha_2)\boldsymbol{k}\otimes\boldsymbol{k} + (\alpha_1 - 3\alpha_2)\boldsymbol{l}\otimes\boldsymbol{l} - 2\alpha_1\boldsymbol{m}\otimes\boldsymbol{m}\right]. \end{aligned} \quad (4.2)$$

– Uniform shear in the plane spanned on $\boldsymbol{m}$ and $\boldsymbol{k}$, i.e., $\boldsymbol{\sigma} = \tau_0(\boldsymbol{m}\otimes\boldsymbol{k} + \boldsymbol{k}\otimes\boldsymbol{m})$, $\tau_0 > 0$. From (3.16) and (3.17) we get

$$J_m = I_{3m} = 0, \quad I_{4m} = \tau_0^2, \quad \dot{\boldsymbol{\varepsilon}}^{cr} = \frac{\sqrt{3\alpha_3}}{2}\dot{\varepsilon}_{\mathrm{eq}}(\boldsymbol{m}\otimes\boldsymbol{k} + \boldsymbol{k}\otimes\boldsymbol{m}). \quad (4.3)$$

The next step is the form of the creep potential $W(\sigma_{\mathrm{eq}})$ or the form of the creep rate versus stress dependence in the steady-state range. The criteria for the choice of a suitable function are the type of the deformation mechanisms operating for the given stress and temperature range as well as the best fitting of the experimentally obtained strain versus time curves. Experimental data for the weld metal 9CrMoNbV are presented in [18] for the stress range 87–100 MPa and constant temperature 650°C. The authors of [18] used a power law to fit experimental data for secondary creep of longitudinal and transverse specimens. In this case the Norton–Bailey–Odqvist creep potential can be applied [27]:

$$W(\sigma_{\mathrm{eq}}) = \frac{a}{n+1}\sigma_{\mathrm{eq}}^{n+1}, \quad \dot{\varepsilon}_{\mathrm{eq}} = a\sigma_{\mathrm{eq}}^n, \quad (4.4)$$

where a and n are material constants. For the longitudinal direction from (4.1) and (4.4) follows

$$\dot{\varepsilon}_L^{\mathrm{cr}} \equiv \boldsymbol{m}\cdot\dot{\boldsymbol{\varepsilon}}^{\mathrm{cr}}\boldsymbol{m} = a_L\sigma_0^n, \quad a_L \equiv a\alpha_1^{\frac{n+1}{2}}. \quad (4.5)$$

Taking the longitudinal direction to be the "reference" direction, we set in (4.5) $\alpha_1 = 1$. From (4.2) and (4.4) we obtain for the transverse direction

$$\dot{\varepsilon}_T^{cr} \equiv \boldsymbol{k}\cdot\dot{\boldsymbol{\varepsilon}}^{cr}\cdot\boldsymbol{k} = a_T\sigma_0^n, \quad a_T \equiv a\left(\frac{1+3\alpha_2}{4}\right)^{\frac{n+1}{2}}. \quad (4.6)$$

In [18] the values for material constants are presented. However, the exponent n is found to be different for longitudinal and transverse directions. Different values for n contradict the creep potential hypothesis employed in the previous section. Here we compute the values for a_L, a_T, and n based on the following functional:

$$\begin{aligned} &F(\tilde{a}_L, \tilde{a}_T, n) = \sum_{i=1}^{k}(\tilde{a}_L + n\tilde{\sigma}_i - \tilde{\dot{\varepsilon}}_{L_i})^2 + \sum_{i=1}^{k}(\tilde{a}_T + n\tilde{\sigma}_i - \tilde{\dot{\varepsilon}}_{T_i})^2, \\ &\tilde{a}_L \equiv \log\, a_L, \quad \tilde{a}_T \equiv \log\, a_T, \quad \tilde{\sigma} \equiv \log\sigma_0, \quad \tilde{\dot{\varepsilon}}_L \equiv \log\, \dot{\varepsilon}_L, \quad \tilde{\dot{\varepsilon}}_T \equiv \log\, \dot{\varepsilon}_T, \end{aligned} \quad (4.7)$$

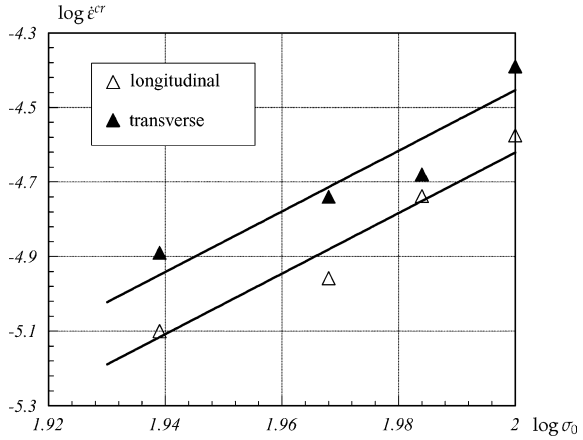

Fig. 8 Minimum creep rates versus stress (experimental data after [18])

where k is the number of experimental data points. Setting the first variation of F equal to zero leads to the system of three algebraic equations with respect to $\tilde{a}_L$, $\tilde{a}_T$, and n. As the result we obtain the following set of material constants:

$$a_L = 1.377 \times 10^{-21}\text{MPa}^{-n}/\text{h}, \quad a_T = 2.023 \times 10^{-21}\text{MPa}^{-n}/\text{h} \quad n = 8.12. \tag{4.8}$$

Figure 8 shows the experimental data presented in [18] and numerical predictions by use of (4.5), (4.6), and (4.8).

Finally, let us summarize the constitutive equation for secondary creep and the set of identified material constants as follows:

$$\begin{aligned}
&\dot{\boldsymbol{\varepsilon}}^{\text{cr}} = \frac{3}{2} a \sigma_{\text{eq}}^{n-1} \left[J_m \left(\boldsymbol{m} \otimes \boldsymbol{m} - \frac{1}{3} \boldsymbol{I} \right) + \alpha_2 \boldsymbol{s}_p + \alpha_3 (\boldsymbol{\tau}_m \otimes \boldsymbol{m} + \boldsymbol{m} \otimes \boldsymbol{\tau}_m) \right], \\
&\sigma_{\text{eq}}^2 = \left(\boldsymbol{m} \cdot \boldsymbol{\sigma} \cdot \boldsymbol{m} - \frac{1}{2} \text{tr}\, \boldsymbol{\sigma}_p \right)^2 + \frac{3}{2} \alpha_2 \text{tr}\, \boldsymbol{s}_p^2 + 3\alpha_3 \tau_{\boldsymbol{m}}^2, \\
&a = 1.377 \times 10^{-21}\text{MPa}^{-n}/\text{h}, \quad n = 8.12, \quad \alpha_2 = 1.117.
\end{aligned} \tag{4.9}$$

5 Conclusions

Creep and damage behaviors of a multipass weld are primarily determined by the arrangement of columnar, coarse-grained, and fine-grained zones within the weld beads. The anisotropic creep of the weld metal is related to different mechanisms of the stress redistribution between the constituents for different loading directions. The results of the uniaxial model developed for binary media confirm this fact and agree qualitatively with experimental observations.

To develop a model for secondary creep under multiaxial stress states, the weld metal is assumed to behave as a quasihomogeneous transversely isotropic solid. The outcome is the coordinate-free equation for secondary creep (4.9) formulated in terms of the Norton–Bailey–Odqvist creep potential and three invariants of the stress deviator. Based on the experimental data presented in [18], the material constants are identified. The weighting factor α_3, which stands for the influence of the transverse shear stress, remains undetermined in (4.9). Future work should be directed toward the understanding of creep and damage mechanisms in weld metals and related testing under stress states with nonzero vector $\boldsymbol{\tau}_m$.

The model (4.9) is limited only to secondary creep behavior and allows one to reproduce only the secondary part of the creep curves presented in [18]. For the description of the whole creep process including the primary and tertiary creep stages, the model (4.9) must be modified by use of hardening and damage variables. The extension and validation of the model will be discussed in a forthcoming paper.

References

1. Altenbach, H., Altenbach, J., Kissing, W.: Mechanics of Composite Structural Elements. Springer, Berlin Heidelberg New York (2004)
2. Altenbach, H., Altenbach, J., Zolochevsky, A.: Erweiterte Deformationsmodelle und Versagenskriterien der Werkstoffmechanik. Deutscher Verlag für Grundstoffindustrie, Stuttgart (1995)
3. Altenbach, H., Huang, C., Naumenko, K.: Creep damage predictions in thin-walled structures by use of isotropic and anisotropic damage models. J Strain Anal **37**, 265–275 (2002)
4. Altenbach, H., Kushnevsky, V., Naumenko, K.: On the use of solid- and shell-type finite elements in creep-damage predictions of thinwalled structures. Arch Appl Mech **71**, 164–181 (2001)
5. Altenbach, H., Naumenko, K., Zhilin, P.: A note on transversely isotropic invariants. ZAMM DOI 10.1002/zamm.200510227, pp. 1–7
6. Altenbach, H., Naumenko, K., Zhilin, P.: A micro-polar theory for binary media with application to phase-transitional flow of fiber suspensions. Continuum Mech Thermodyn **15**, 539–570 (2003)
7. Aurich, D., Kloos, K.H., Lange, G., Macherauch, E.: Eigenspannungen und Verzug durch Wärmeeinwirkung, DFG Forschungsbericht. Wiley-VCH, Weinheim (1999)
8. Bertram, A., Olschewski, J.: A phenomenological anisotropic creep model for cubic single crystals. In: Lemaitre, J. (ed.) Handbook of Material Models, pp. 303–307. Academic, San Diego (2001)
9. Betten, J.: Creep Mechanics. Springer, Berlin Heidelberg New York (2002)
10. Boehler, J.P.: Representations for isotropic and anisotropic non-polynomial tensor functions. In: Boehler, J.P. (ed.) Applications of Tensor Functions in Solid Mechanics, pp. 31–53. Springer, Berlin Heidelberg New York (1987)
11. Bruhns, O., Xiao, H., Meyers, A.: On representation of yield functions for crystals, quasicrystals and transversely isotropic solids. Eur J Mech A/Solids **18**, 47–67 (1999)
12. Chawla, K.K.: Composite Materials. Springer, Berlin Heidelberg New York (1987)
13. Courant, R., Hilbert, D.: Methods of Mathematical Physics, Partial Differential Equations, vol. 2. Wiley Interscience, New York (1989)
14. Eggeler, G., Rametke, A., Coleman, M., Chew, B., Peter, G., Burblies, A., Hald, J., Jefferey, C., Rantala, J., deWitte, M., Mohrmann, R.: Analysis of creep in a welded P91 pressure vessel. Int J Pres Ves Piping **60**, 237–257 (1994)
15. Hall, F.R., Hayhurst, D.R.: Continuum damage mechanics modelling of high temperature deformation and failure in a pipe weldment. Proc R Soc Lond A **433**, 383–403 (1994)
16. Hayhurst, D.R.: The use of continuum damage mechanics in creep analysis for design. J Strain Anal **25**, 233–241 (1994)
17. Hayhurst, D.R., Wong, M.T., Vakili-Tahami, F.: The use of CDM analysis techniques in high temperature creep failure of welded structures. JSME Series A **45**, 90–97 (2002)
18. Hyde, T.H., Sun, W., Agyakwa, P.A., Shipeay, P.H., Williams, J.A.: Anisotropic creep and fracture behaviour of a 9CrMoNbV weld metal at 650°C. In: Skrzypek, J.J., Ganczarski, A.W. (eds.) Anisotropic Behaviour of Damaged Materials, pp. 295–316. Springer, Berlin Heidelberg New York (2003)
19. Hyde, T.H., Sun, W., Becker, A.A., Williams, J.A.: Creep continuum damage constitutive equations for the base, weld and heat-affected zone materials of a service-aged 1/2Cr1/2Mo1/4V:2 1/4Cr1Mo multipass weld at 640°C. J Strain Anal **32**, 273–285 (1997)
20. Hyde, T.H., Sun, W., Williams, J.A.: Creep behaviour of parent, weld and HAZ materials of new, service aged and repaired 1/2Cr1/2Mo1/4V: 21/4Cr1Mo pipe welds at 640°C. Mater High Temp **16**, 117–129 (1999)
21. Hyde, T.H., Sun, W., Williams, J.A.: Creep analysis of pressurized circumferential pipe weldments—a review. J Strain Anal **38**, 1–29 (2003)
22. Kowalewski, Z.: The role of grain size on creep of copper under uniaxial tension. Arch Metall **37**, 65–76 (1992)
23. Leckie, F.A., Hayhurst, D.R.: Constitutive equations for creep rupture. Acta Metall **25**, 1059–1070 (1977)
24. Lundin, C.D., Liu, P., Prager, M.: Creep behavior of weld heat affected zone regions for modified 9Cr-1Mo Steel. In: Proceedings of CREEP7, pp. 379–436. Japan Society of Mechanical Engineers, Tsukuba (2001)
25. Matsui, M., Tabuchi, M., Watanabe, T., Kubo, K., Kinugawa, J., Abe, F.: Degradation of creep strength in welded joint of 9%Cr steel. ISIJ Int **41**, S126–S130 (2001)
26. Nabarro, F.R.N., de Villiers, H.L.: The Physics of Creep. Creep and creep-resistant alloys. Taylor and Francis, London (1995)
27. Odqvist, F.K.G., Hult, J.: Kriechfestigkeit metallischer Werkstoffe. Springer, Berlin Heidelberg New York (1962)
28. Robinson, D.N., Binienda, W.K., Ruggles, M.B.: Creep of polymer matrix composites. I: Norton/Bailey Creep Law for transverse isotropy. J Eng Mech ASCE **129**, 310–317 (2003)
29. Shibli, I.A.: Performance of P91 thick section welds under steady and cyclic loading conditions: power plant and research experience. OMMI 1. Available at http://www.ommi.co.uk (2002)
30. Wohlfahrt, H., Brinkmann, D.: Consideration of inhomogeneties in application of deformation models, describing the inelastic behaviour of welded joints. In: Steck, E., Ritter, R., Peil, U., Ziegenbein, A. (eds.) Plasticity of Metals: Experiments, Models, Computation. Final report of the Collaborative Research Centre 319, Stoffgesetze für das inelastische Verhalten metalischer Werkstoffe—Entwicklung und technische Anwendung, pp. 361–382. Wiley-VCH, Weinheim (2001)
31. Wu, R., Sandström, R., Seitisleam, F.: Influence of extra coarse grains on the creep properties of 9 percent CrMoV (P91) steel weldment. Trans ASME J Eng Mater Technol **26**, 87–94 (2004)